Nanoscale Advances

ROYAL SOCIETY OF CHEMISTRY

PAPER

View Article Online
View Journal | View Issue

Cite this: *Nanoscale Adv.*, 2024, **6**, 1556

Improvements in properties of polybenzoxazine-based laser-induced graphene (LIG) by alloying with polyimide and modeling of production process

Ibrahim Lawan,[a] Panuwat Luengrojanakul,[a] Krittapas Charoensuk,[a] Hariharan Argunam,[b] Cheol-Hee Ahn[c] and Sarawut Rimdusit *[a]

Laser-induced graphene (LIG) is conventionally produced from polyimide among thermosetting polymer substrates, but its flexible nature limits its tremendous potential in applications where flexibility of the substrate is not desired. Interestingly, polybenzoxazine has also been found to have potential as a substrate in LIG production. However, aside from being brittle, it has inferior char residue and thermal stability relative to polyimide, which could result in the production of LIG with inferior properties. Thus, exploring possible improvements in the properties of the polybenzoxazine-based substrate and LIG by alloying with polybenzoxazine and polyimide is the major motivation of this study. First, the improvement in the toughness, char residue and thermal stability of polybenzoxazine by alloying with polyimide was explored. Second, the properties of a LIG obtained from the polybenzoxazine/polyimide alloy were studied. The electrical sheet resistivity, Raman spectra indices, structural morphologies, and crystal size of the neat polybenzoxazine and polybenzoxazine/polyimide alloy substrates were compared. The results reveal significant improvements in the electrical resistivity, structural morphology, and crystal size of the LIG. In addition, the improved polybenzoxazine/polyimide alloy substrate was used to optimize the operational parameters of the laser machine for the production of the LIG. LIG with a minimum electrical sheet resistivity of 3.61 Ω sq^{-1}, multi-layer crystals as confirmed by Raman spectroscopic analysis, and a sponge-like highly porous structure was achieved with the optimum operational conditions in an ambient environment. Last, a quadratic model was found and validated to suitably define the production process. The study demonstrated an improvement in the property of a rigid polybenzoxazine-based LIG by alloying polybenzoxazine with polyimide for the first time.

Received 21st November 2023
Accepted 6th February 2024

DOI: 10.1039/d3na01026k

rsc.li/nanoscale-advances

Introduction

Nanomaterials are among the most versatile materials in the world, with applications cutting across various fields of human endeavour. Structurally, nanomaterials are grouped into four categories, namely carbon-based, organic, inorganic, and composite.[1] Graphene is among carbon-based nanomaterials formed by a layer of sp^2-hybridized carbon atoms arranged into a 2D-dimensional honeycomb-like lattice structure. It is applied in the field of energy storage, composite development, electronics, photonics, medical, and environmental management, for its high surface area and Young's modulus, excellent thermal stability, excellent electrical conductivity, and ultra-high electron mobility.[2,3] Traditionally, graphene is synthesized using mechanical and liquid exfoliation, chemical vapour deposition, and flash joule heating. However, the aforementioned methods have been reported to be tedious, high-energy consuming and low productivity.[3]

In 2014, laser-induced graphene (LIG) production emerged, and since then the technique has been proved to be a versatile and efficient alternative method with very high precision and reduced capital expenditure.[4] In addition, it has the advantages of producing high-surface-area graphene with a single production step with no chemical additives, agents, or solvents.[5,6] Recently, Lawan *et al.*[7] outlined major steps taken in the production of LIG using a thermosetting polymer substrate, namely, polymer substrate preparation, specification of laser machine parameters, application of the laser-induced irradiation on the prepared substrate, and characterization of the obtained LIG.

First, with regards to thermosetting polymer substrates, different polymers have been used as substrates in LIG production. Polyimide is conventionally used among

[a]*Chulalongkorn University Faculty of Engineering, Thailand. E-mail: Sarawut.R@chula.ac.th*
[b]*PSG Institute of Technology and Applied Research, India*
[c]*Seoul National University, Korea*

different research groups, perhaps due to its high thermal stability and char residue characteristics.[7] The high thermal stability and char residue characteristics are attributed to the stacked aromatic hydrocarbon in its structure.[8–10] It is mostly used in the production of LIG for application in the areas of wearable and flexible electronics, where substrate flexibility is an advantage.[11,12] However, the flexibility of the polyimide substrate will definitely limit the application of the polyimide-based LIG where rigidity is desired. Luong *et al.*[13] corroborated this assertion where it was established that the type of substrate used could limit the applications of the resulting LIG. In addition, an independent research group hypothesized that flexible substrate-based LIG is susceptible to damage through mechanical abrasion and demonstrated a concept of laminating an LIG composite to avert damage.[14] Moreover, polyimide substrate curing is very tricky as a curing agent is needed for appreciable low-temperature curing.[15,16]

Interestingly, new phenolic resins known as polybenzoxazines, which are obtained from the ring-opening polymerization of benzoxazine monomers, emerged. Apart from their rigidity and mechanical performance, polybenzoxazines have an easy and environmentally friendly polymerization reaction, molecular design flexibility, near-zero shrinkage upon curing, and low water absorption.[17–19] However, aside from being brittle, polybenzoxazines have inferior thermal properties and char residue relative to polyimide and that could result in the production of a brittle substrate and LIG with inferior properties compared to LIG produced from a polyimide-based substrate. Thus, this presents a challenge of improving the polybenzoxazine substrate to have higher thermal stability and char residue, in addition to possible improvement in toughness for applications that require a tough and rigid substrate without extra support and protection. A study demonstrated blending polybenzoxazine with polyimide to produce a substrate with improved thermal stability and char residue. Therein, bisphenol-A polybenzoxazine with around 35% char residue was alloyed with polyimide and results showing some positive trends have been presented.[17] However, the actual improvement of the thermal stability and char residue by alloying polybenzoxazine and polyimide and whether the magnitude of the improvements could positively influence the properties of the LIG, have not been reported.

Second, the laser machine used in the production of the LIG has parameters such as laser power, scanning speed, focus distance, and pulse per inch (PPI), which were found to have tremendous influence on the LIG production.[20–22] Ming *et al.*[21] mentioned laser power and scanning speed as the foremost parameters affecting LIG production, and several preliminary experimental runs conducted in this study confirmed that the laser power and engraving speed are the most significant factors affecting LIG production. Considering how numerous the aforementioned parameters are and the various levels in which each could be adjusted for efficient LIG production, the need for optimization of the parameters for the production of LIG with desirable properties for any interesting substrate cannot be over-emphasized. Unfortunately, according to literature reports, the optimization process is usually done by manual manipulation of the parameters and their levels. Interestingly, Wahab *et al.*[23] and Pinheiro *et al.*[24] recently demonstrated some improved methods of optimizing LIG production from substrates, namely Bayesian and pulse modulation operation optimization methods, for the production of LIG from graphene oxide/polyimide-based and paper-based substrates, respectively. Hitherto, optimization of LIG production from a polybenzoxazine/polyimide alloy substrate has not been reported, despite of its potential, to the best of our knowledge.

Therefore, this study focused on achieving the following objectives.: (i) to determine the improvements in toughness, thermal stability and char residue of polybenzoxazine by alloying with polyimide, (ii) to determine whether the improvements in thermal stability and char residue achieved in (i) could influence improvements in the properties of the LIG produced, and (iii) to optimize and model the alloy-based LIG production process using the central composite design (CCD) package of response surface methodology (RSM).

Experimental

Materials used

Analytical-grade phenol and paraformaldehyde were purchased from Loba Chemie Pvt. Ltd, India and Merck, Darmstadt, Germany, respectively, while 3,3,4,4-biphenyltetracarboxylic dianhydride (s-BPDA), 1,4,5,8-naphthalenetetracarboxylic dianhydride (NTDA), 4,4′-oxydianiline (ODA), and *N*-methyl-2-pyrrolidinone (NMP) were purchased from Tokyo Chemical Industry (TCI), Tokyo.

Preparation of the polybenzoxazine/polyimide alloy substrate

First, polybenzoxazine resin was synthesized by the solventless procedure by combining phenol, ODA, and paraformaldehyde in a 2 : 1 : 4 molar ratio, as depicted in Scheme 1. The reaction mixture was heated at 130 °C for 2 hours to obtain a deep yellow solid denoted as Ph-dde resin. Second, polyamic acid was synthesized by mixing ODA, NTDA, and BPDA in a 1 : 0.5 : 0.5 molar ratio with an NMP solvent of approximately four times weight of the formulation for 5 hours (Scheme 2). Last, prepared Ph-dde resin was ground to a fine powder. Then, it was slightly heated for liquefaction before diluting it with some quantity of NMP to aid mixing. The liquefied Ph-dde resin was mixed with synthesized polyamic acid in 70 : 30 and 50 : 50 weight ratios of Ph-dde and polyamic acid (Scheme 3), respectively. Then, 100 : 0, 70 : 30, 50 : 50, and 0 : 100 formulations were poured differently into silicon moulds. The silicon moulds containing the

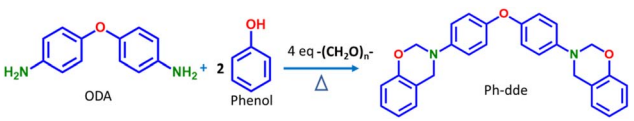

Scheme 1

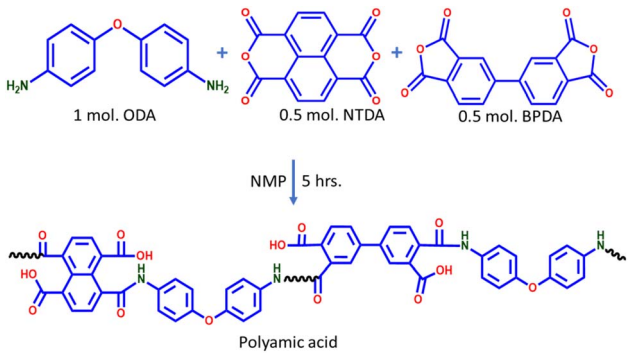

Scheme 2

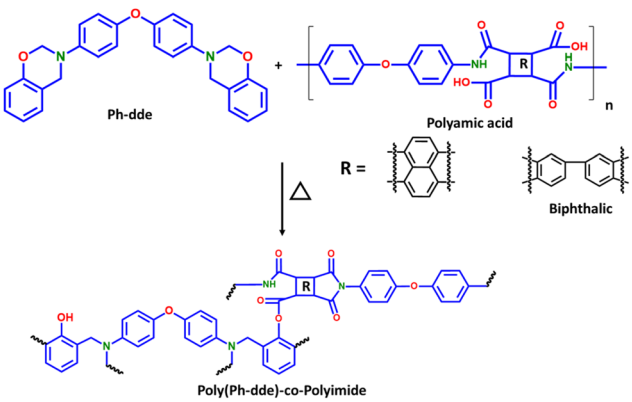

Scheme 3

formulations were heated at; 80 °C for 12 hours to evaporate off the NMP solvent used in the formulations. This is followed by step curing as follows; 120 to 150 °C at 10 °C increment for 1 hour each and 160 to 240 °C at 20 °C increment for 2 hours each. Heating of the Ph-dde resin (100 : 0) was stopped at 200 °C, while the formulations (70 : 30 and 50 : 50) and the polyamic acid (0 : 100) were removed from silicon moulds to finish heating at 240 °C in aluminium foil cups to prevent damaging the silicon moulds. The samples obtained after the curing are denoted as 100%poly(Ph-dde),70%poly(Ph-dde) : 30%polyimide, 50%poly(Ph-dde) : 50%polyimide, and 100% polyimide.

The obtained substrates were characterized using Fourier-transform infrared spectroscopy (FTIR), differential scanning calorimeter (DSC) thermograms, thermogravimetry, and toughness (flexural stress and strain analysis, ASTM D79-M93) using a spectrometer (Spectrum GX, PerkinElmer), a DSC (DSC module 1, Mettler-Toledo), a thermogravimetric analyzer (GC10, Mettler-Toledo), and a universal testing machine (Instron 5567), respectively.

Production of graphene on the prepared substrate using a laser machine

Laser-induced graphene (LIG) with dimensions of 5 mm by 5 mm was produced by single passage engrave using a Trotec Laser Machine (Speedy 100/R-C8063) on the 100%poly(Ph-dde) and 50%poly(Ph-dde) : 50%polyimide substrates. The machine was operated in ambient air with power, speed, pulse per inch (PPI), and focus parameters set at 4.5 W, 18 cm S^{-1}., 1000 and 1.5 inches, respectively. The LIG produced from different substrates were characterized by measuring the sheet resistance and crystal size (eqn (1)) using four-point probe equipment (Jandel RM3) with a bias current of 1 mA and a Raman spectrometer, respectively.

$$L_a(\text{nm}) = (2.4 \times 10^{-10}) \times \lambda_l^4 \times \left(\frac{I_D}{I_G}\right)^{-1} \quad (1)$$

where L_a = crystal size (nm), λ = 532 nm, $\frac{I_D}{I_G}$ to be obtained from Raman spectra obtained from the Raman spectroscopic analysis.

Modeling and optimization of the LIG production

Response surface methodology (RSM) has the advantage of using fewer experimental runs to reliably understand the effects of factors and their interactions on the response.[25] Therefore, that was the basis for the selection of the central composite design (CCD), which is a sub-set of the RSM, for the modeling and optimization of the LIG production using the polybenzoxazine/polyimide alloy substrate. After a series of preliminary experimental runs with the alloy substrate, 1.5 and 12 W laser power, and 9 and 36 cm s^{-1} laser engraving speed, extreme operating conditions (lowest and highest values, respectively) were established and inputted into the Design Expert Software (Version 12). The PPI and focus were maintained as 1000 and 1.5 inches, respectively. The laser machine was operated under ambient environmental conditions throughout. Table 1 presents the experimental runs required to achieve the objective, and each run was repeated three times, and the average values of responses were inputted into the software for analysis. The respective response (sheet resistance (Ω sq^{-1})) of each LIG sample was measured using four-point probe equipment (Jandel, RM3) with a bias current of 1 mA.

Table 1 Experimental design and values of response

Experimental run	Factor *A*: power (W)	Factor *B*: speed (cm s^{-1})	Response: sheet resistance (Ω sq^{-1})
1	3.0	22.5	30.4
2	13.9	22.5	22.0
3	3.0	9.0	26.8
4	12.0	9.0	8.0
5	12.0	36.0	14.0
6	7.5	3.4	6.0
7	3.0	36.0	14.0
8	7.5	41.6	4.1
9	7.5	22.5	5.5
10	7.5	22.5	4.0
11	7.5	22.5	3.9
12	7.5	22.5	3.8
13	7.5	22.5	3.7

Results and discussion

Prepared polybenzoxazine/polyimide alloy substrate

Fig. 1(a) depicts the DSC thermograms of substrate samples; as it can be observed, no exothermic peak appeared in any of the samples, indicating that the step curing within the temperature range used has appreciably cured the substrates. Fig. 1(b) presents the FTIR spectra of the samples; noticeable absorption peaks due to the tetra-substituted benzene ring and hydrogen linked to the phenol OH can be seen at 1487 and 1622 cm^{-1}, indicating that the linking due to Mannich bridging by ring-opening polymerization has occurred. Furthermore, absorption at 1778 cm^{-1}, which is due to the C=O vibration of polyimide, could be observed with the 100%polyimide, 50%poly(Ph-dde) : 50%polyimide, and 30%poly(Ph-dde) : 70%polyimide substrates, which confirms imization of the substrates. These findings are comparable with the findings reported for a similar system.[17] Thus, appreciably cured polybenzoxazine/polyimide alloy substrate and the neat (100%poly(Ph-dde) and 100%polyimide) samples have been achieved.

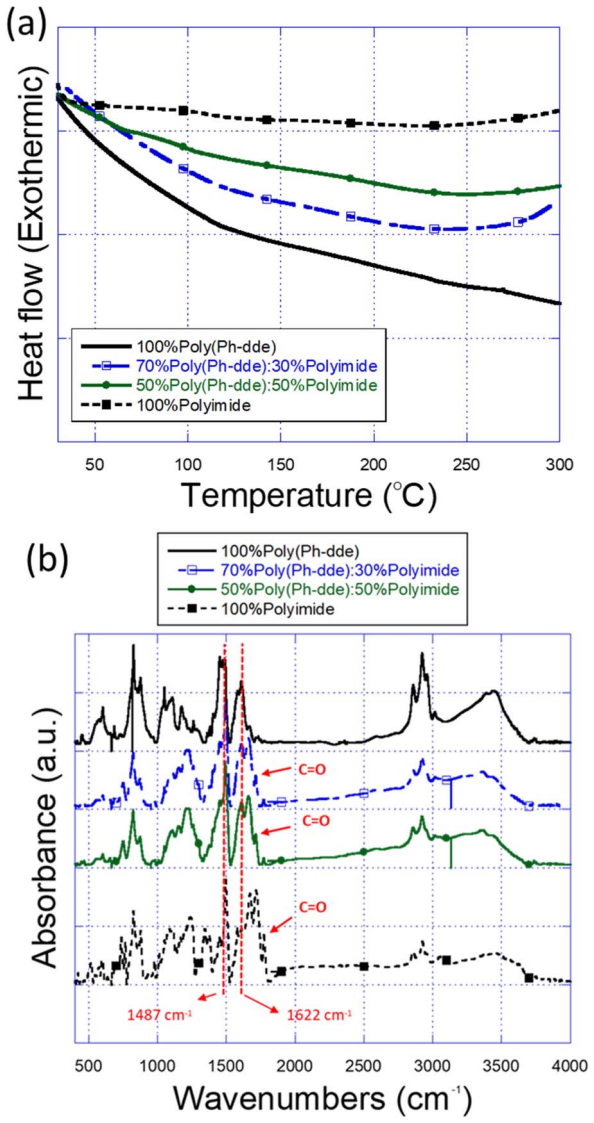

Fig. 1 Characteristics of cured substrates: DSC thermograms (a) and FTIR (b).

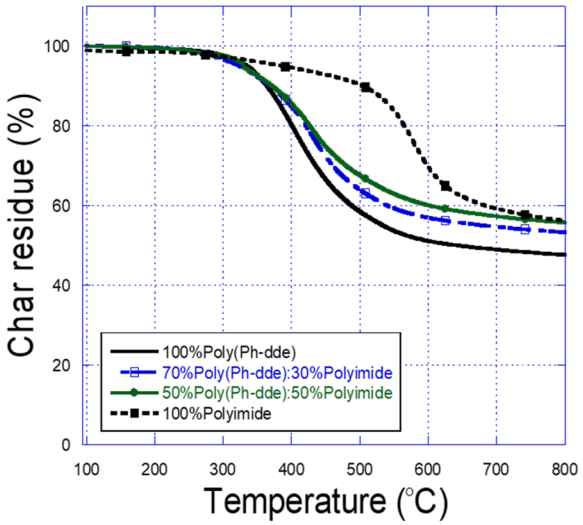

Fig. 2 Thermogravimetric analysis of the substrates.

Fig. 2 depicts the thermal stability and char residue results recorded from the TGA of cured substrates. The 100%poly(Ph-dde) substrate exhibited the lowest thermal stability and char residue, while the 100%polyimide substrate exhibited the highest thermal stability and char residue. An obvious increase in thermal stability and char residue is achieved with the increase in the amount of polyimide in the polybenzoxazine/polyimide alloy system.

Table 2 presents the thermal degradation temperatures (T_{d5} and T_{dmax}) and char residue (CR) of substrate samples. With 50 wt% polyimide in the alloy, a slight increase in the T_{d5} and a substantial increase in the T_{dmax} (+23 °C) was achieved. Similarly, a significant increase in the CR (~17% increase) was achieved, giving the 50%poly(Ph-dde) : 50%polyimide alloy substrate a CR that almost matches that of the 100%polyimide substrate. These improvements could be directly linked to the high thermal stability and CR of polyimide, which are attributed to its rich aryl hydrocarbon structure. The 50%poly(Ph-dde) : 50%polyimide, with the highest thermal stability and char residue that almost match those of the 100%polyimide, represents the best polybenzoxazine/polyimide alloy substrate for LIG production.

Fig. 3 presents flexural stress *versus* strain plots and toughness of the 100%poly(Ph-dde),70%poly(Ph-dde) : 30%polyimide

Table 2 Thermogravimetric data for the substrates

Sample	T_{d5} (°C)	T_{dmax} (°C)	Char residue (%)
100%poly(Ph-dde)	327	408	47.8
70%poly(Ph-dde) : 30%polyimide	328	422	53.4
50%poly(Ph-dde) : 50%polyimide	329	431	56.0
100%polyimide	389	580	56.3

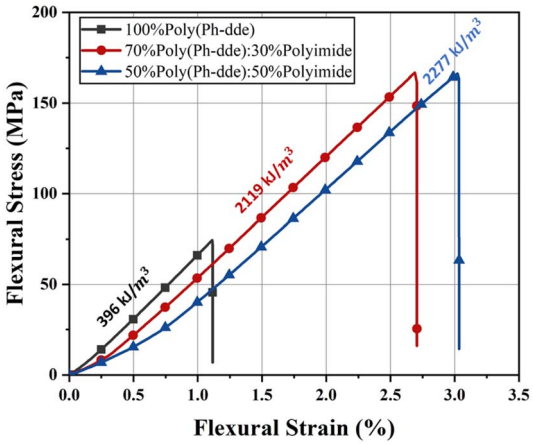

Fig. 3 Flexural stress–strain plots and toughness of the substrates.

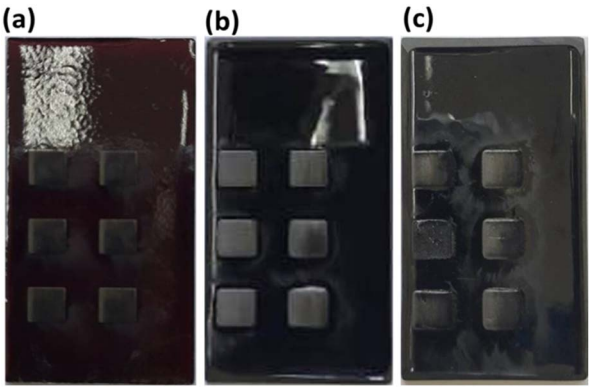

Fig. 4 Images of the LIG: 100%poly(Ph-dde)-LIG (a), 50%poly(Ph-dde) : 50%polyimide-LIG (b), and 50%poly(Ph-dde) : 50%polyimide-LIG produced using the optimum conditions (c).

and 50%poly(Ph-dde) : 50%polyimide substrates. The toughness of the 100%polyimide could not be established because its flexibility made it unsuitable for the flexural test used. It could be observed that significant improvement in the toughness of the polybenzoxazine/polyimide alloy compared to neat polybenzoxazine substrate was achieved. Improvement in toughness by about four times was achieved with the 50%poly(Ph-dde) : 50%polyimide substrate.

Produced LIG on the prepared substrate

Fig. 4 presents images of the produced 5 mm by 5 mm LIG samples engraved on the 100%poly(Ph-dde) (Fig. 4(a)) and 50% poly(Ph-dde) : 50%polyimide (Fig. 4(b)).

Fig. 5(a) and (b) show Raman spectra of the LIG samples the three characteristics peaks, D, G, and 2D at 1350 cm^{-1}, 1580 cm^{-1}, and 2680 cm^{-1}, respectively are shown on the Raman spectra, which confirms the production of graphene on both the substrates. The D peak is linked to disorders and defects in the graphene structure, while G and 2D peaks are due to carbon atom vibration because of the sp^2 hybridization in the hexagonal lattice and stacking and phonon of the graphene structure, respectively.[26–29] It could be observed that the D peak

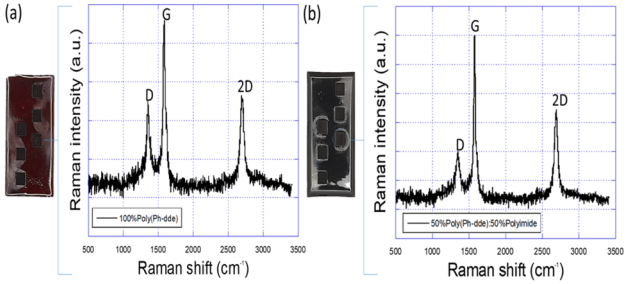

Fig. 5 Raman spectra of the LIG: 100%poly(Ph-dde)-LIG (a) and 50% poly(Ph-dde) : 50%polyimide-LIG (b).

intensity in the 100%poly(Ph-dde)-LIG spectrum (Fig. 5(a)) is much more pronounced relative to the D peak intensity in the 50%poly(Ph-dde) : 50%polyimide-LIG spectrum (Fig. 5(b)). Consequently, higher $\frac{I_D}{I_G}$ was recorded with the 100%poly(Ph-dde)-LIG (Table 3), suggesting that the 50%poly(Ph-dde) : 50% polyimide-LIG has less disorders and defects compared to the 100%poly(Ph-dde)-LIG. Additionally, the 50%poly(Ph-dde) : 50%polyimide-LIG had a higher $\frac{I_{2D}}{I_G}$ (Table 3), which suggests a higher stacking order of the graphene structure.

Similarly, the L_a of the 50%poly(Ph-dde) : 50%polyimide-LIG was found to be significantly higher than that of the 100% poly(Ph-dde)-LIG (Table 3), where an increase of about 61% was achieved. This is owing to the fact that L_a is inversely related to the $\frac{I_D}{I_G}$. This improvement also implies that the 50%poly(Ph-dde) : 50%polyimide-LIG has a more porous structure, as it has been established that graphene structures with larger L_a possess more porous structures.[29] Moreover, a significantly lower electrical resistivity was recorded with the 50%poly(Ph-dde) : 50% polyimide-LIG (Table 3), compared to that of the 100%poly(Ph-dde)-LIG, with a reduction in electrical resistivity of about 37% being achieved. This finding further corroborates the improvement in porosity, as it has been established that higher porosity in LIG structures leads to lower electrical resistivity, as electrical resistivity arises from hopping of carriers between crystals.[29]

Observation of the surface morphology of the LIG samples (100 μm scale images in Fig. 6) reveals a ridge-like route indicating laser engraving passages, with the 50%poly(Ph-dde) : 50%polyimide-LIG exhibiting a much more pronounced ridge-like route, which could be attributed to the higher stability and char yield of the substrate. Thermosetting polymer substrate-based LIG has been reported to have similar engraving passages route.[30,31] Moreover, spots believed to be structural disorder and defects were observed in both the LIG samples. However, more and bigger spots were observed with the 100%poly(Ph-dde)-LIG (Fig. 6(a)), and a zoomed-in image (10 μm per scale) of the spots shows structural collapse in the graphene structures, which is contrary to the case of the 50% poly(Ph-dde) : 50%polyimide-LIG (Fig. 6(b). This observation is in agreement with the trend of results presented in Table 3.

Table 3 Properties of the LIG

Sample	Sheet resistance (Ω sq^{-1})	Raman spectra indices $\frac{I_D}{I_G}$	$\frac{I_{2D}}{I_G}$	L_a (nm)
100%poly(Ph-dde)-LIG	28.08 ± 1.2	0.53	0.47	36.3
50%poly(Ph-dde) : 50%polyimide-LIG	17.67 ± 1.8	0.33	0.55	58.3

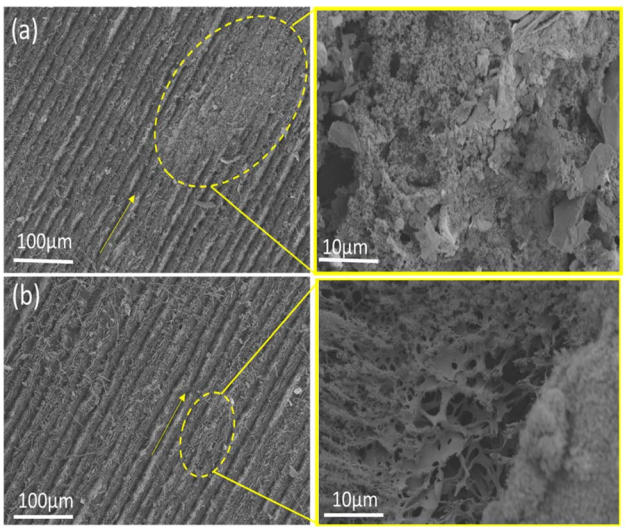

Fig. 6 SEM Images of the LIG: 100%poly(Ph-dde)-LIG (a) and 50% poly(Ph-dde) : 50%polyimide-LIG (b).

Therefore, it can be summarized that the less disorders and defects in the lattice structure, the larger L_a, larger porosity, and lower electrical resistance achieved with the 50%poly(Ph-dde) : 50%polyimide-LIG can be attributed to the relatively higher thermal stability and char yield of the polybenzoxazine/polyimide alloy substrate.

Optimized conditions and model of the LIG engraving on the prepared substrate

Table 1 presents various responses (sheet resistance (Ω sq^{-1})) recorded for each experimental run designed using the 50% poly(Ph-dde) : 50%polyimide substrate. The values ranged from 3.7 to 30.4 Ω sq^{-1}, and further analyses generated plots showing the effects of power (W) and speed (cm s^{-1}) on the sheet resistance (Ω sq^{-1}). Fig. 7(a) and (b) present 3D and contour plots, where the effects of laser power from 3 to 12 W and engraving speed from 9 to 36 cm s^{-1} on the sheet resistance (Ω sq^{-1}) are simultaneously shown. Three distinctive regions could be observed: 3 to 4.6 W *versus* 9 to 16 cm s^{-1}, 5 to 11 W *versus* 18 to 33 cm s^{-1}, and >11 W *versus* >33 cm s^{-1}, marked by orange/green, blue, and green colored regions, were found to have the highest, least, and medium electrical resistance, respectively.

Table 4 presents four relationship templates, and a quadratic model was fitted to the scenario based on the responses recorded from the experimental runs. The quadratic model was found to have adjusted and predicted R^2 values to be closest to 1, and the difference between the adjusted and predicted R^2 is less than 0.2. The model defining the quadratic relationship is presented in eqn (2).

$$\text{Sheet resistance}\left(\frac{\Omega}{\text{Sq.}}\right) = +3.90 - 3.83 \times A - 0.9384 \times B + 4.70 \times AB + 11.08 \times A^2 + 0.8562 \times B^2 \quad (2)$$

Table 5 presents the ANOVA of the quadratic model, where it can be seen that the quadratic model suggested is significant. The laser power was found to be a significant factor, while engraving speed is not significant. In contrast, all model

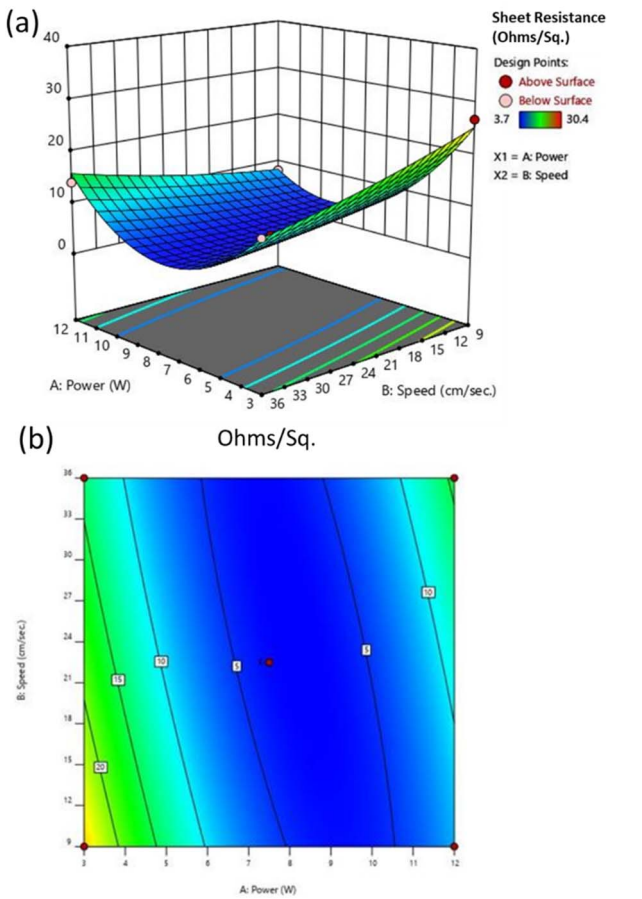

Fig. 7 Plots of the 50%poly(Ph-dde) : 50%polyimide-LIG resistance against power and speed: 3D plot (a) and contour plot (b).

Table 4 Fit summary

Source	Sequential *P*-value	Lack of fit *P*-value	Adjusted R^2	Predicted R^2	Remark
Linear	0.5417	<0.0001	−0.0615	−0.6944	
2FI	0.3634	<0.0001	−0.0704	−0.7787	
Quadratic	<0.0001	0.0002	0.9827	0.9289	Suggested
Cubic	<0.0001	0.0697	0.9994	0.9909	Aliased

Table 5 ANOVA for quadratic model

Source	Sum of squares	df	Mean square	*F*-value	*P*-value	Remarks
Model	1069.73	5	213.95	137.67	<0.0001	Significant
A-power	117.65	1	117.65	75.71	<0.0001	Significant
B-speed	7.04	1	7.04	4.53	0.0708	Not significant
AB	88.36	1	88.36	56.86	0.0001	Significant
A^2	854.22	1	854.22	549.66	<0.0001	Significant
B^2	5.10	1	5.10	3.28	0.1130	Significant
Residual	10.88	7	1.55			
Lack of fit	10.78	3	3.59	143.71	0.0002	Significant
Pure error	0.1000	4	0.0250			
Cor total	1080.61	12				

coefficients (*AB*, A^2 and B^2) were found to be significant. The lack of fit is also significant; however, there is only a 0.02% chance that a lack of fit *F*-value this large could occur due to noise. These findings show that the quadratic model adequately defines the scenario.

Fig. 8 presents a plot of predicted *versus* actual responses, and an obvious linear positive correlation that validates the model is presented as eqn (2).

The software suggests optimum conditions for the production of the 50%poly(Ph-dde) : 50%polyimide-LIG (Fig. 4(c)) to be 8.4 W and 25.2 cm s^{-1} to achieve an electrical sheet resistance of 3.61 Ω sq^{-1}. Findings from the analysis done to validate the optimum conditions revealed a very negligible percentage error between the theoretically suggested optimum sheet resistance and average resistance obtained from repeated experimental runs. Thus, the overall optimum conditions for LIG production using the 50%poly(Ph-dde) : 50%polyimide have been established as 8.4 W, 25.2 cm s^{-1}, 1000 PPI, and 1.5 inches.

Fig. 9 depicts the peaks intensity in the Raman spectrum of the 50%poly(Ph-dde) : 50%polyimide-LIG obtained under the optimum conditions. The D peak is seen to have relatively lower intensity compared to the G and 2D peaks. Consequently, an $\frac{I_D}{I_G}$ as low as 0.29 was recorded, whereas an $\frac{I_{2D}}{I_G}$ as high as 0.74 was

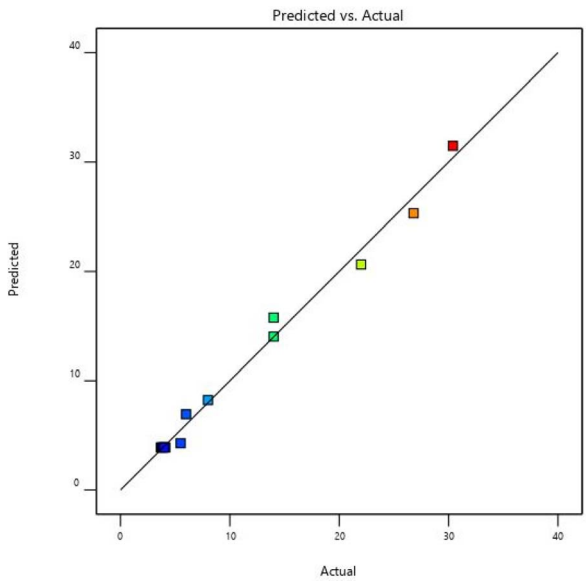

Fig. 8 Quadratic model validation plot.

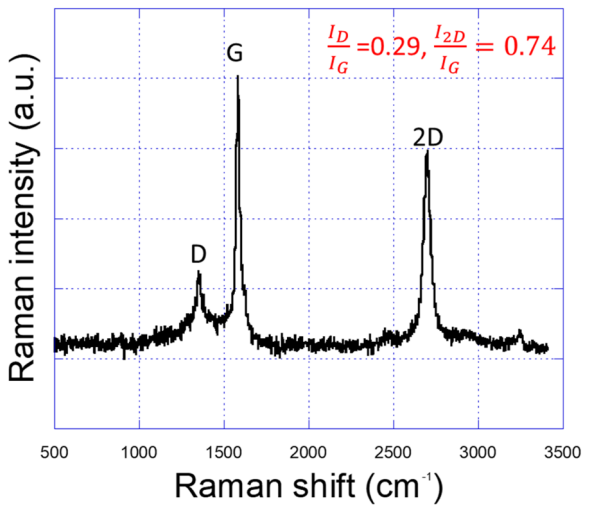

Fig. 9 Raman spectrum of 50%poly(Ph-dde) : 50%polyimide-LIG produced under the optimum conditions.

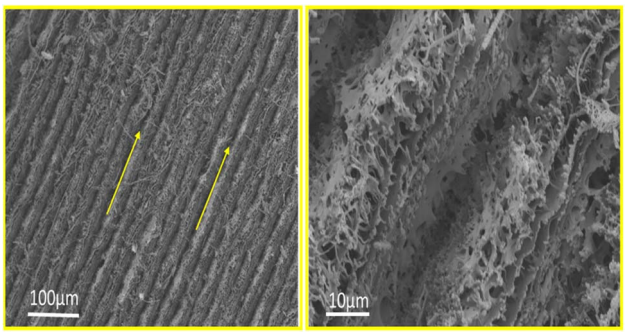

Fig. 10 SEM Images of 50%poly(Ph-dde) : 50%polyimide-LIG produced under the optimum conditions.

recorded. This finding suggests that the graphene produced under the optimum conditions has less disorders and defects.

Conversely, Yu *et al.*[32] stipulated that an $\frac{I_{2D}}{I_G}$ value in the range of 0.72–0.91 indicate the formation of a multi-layered graphene. Thus, this shows that the 50%poly(Ph-dde) : 50% polyimide-LIG produced using the optimum conditions has a multi-layered stacked structure. The values of $\frac{I_D}{I_G}$ and $\frac{I_{2D}}{I_G}$ recorded with the 50%poly(Ph-dde) : 50%polyimide-LIG produced under the optimum conditions compares favourably with the values recorded with LIG produced on a polyimide-based substrate.[33–36] Furthermore, an L_a of 66.3 nm was recorded for the optimum conditions, which shows that the 50% poly(Ph-dde) : 50%polyimide-LIG produced has larger pore spaces compared to the pore spaces of the 50%poly(Ph-dde) : 50%polyimide-LIG (Table 3) produced with power, speed, pulse per inch (PPI), and focus parameters set at 4.5 W, 18 cm s^{-1}, 1000 and 1.5 inches, respectively. Interestingly, the zoomed-in SEM image of the 50%poly(Ph-dde) : 50%polyimide-LIG produced under the optimum conditions (Fig. 10) shows a sponge-like porous structure, which corroborates the findings of low resistance $\frac{I_D}{I_G}$ and high $\frac{I_{2D}}{I_G}$ and L_a achieved with the 50% poly(Ph-dde) : 50%polyimide-LIG.

Conclusion

Based on data recorded, analysis, and discussion presented, the following conclusions could be drawn:

(i) Alloying polybenzoxazine with polyimide has produced a polybenzoxazine-based substrate with significant improvements in toughness, thermal stability, and char residue. For instance, there was a fourfold increase in toughness and increases in thermal degradation and char residue of 23 °C and 17% were achieved, respectively, by alloying with 50 wt% polyimide.

(ii) The aforementioned magnitude of improvements in the substrate has influenced the properties of the LIG produced. A significant reduction in electrical sheet resistance of 37% and a dramatic increase in crystal size of 61% were achieved.

(iii) Laser power and the interaction between laser power and engraving speed were found to significantly affect the properties of the LIG produced.

(iv) A quadratic model was established to adequately define LIG production with the polybenzoxazine/polyimide alloy substrate for the first time. Laser power of 8.4 W and engraving speed of 25.2 cm s^{-1} were established and validated to be optimum parameters to achieve LIG with the lowest electrical resistance of 3.61 Ω sq^{-1}, multi-layer crystals, and a sponge-like highly porous structure.

(v) Overall, the concept of alloying polybenzoxazine with polyimide has produced an improved tough and rigid polybenzoxazine-based substrate for the production of high-performing LIG for applications where a flexible neat polyimide substrate is not desired.

Author contributions

Ibrahim Lawan; conceptualizing, methodology; formal analysis; writing & editing. Panuwat Luengrojanakul; conceptualization; validation. Krittapas Charoensuk; methodology of substrate production. Hariharan Argunam; chemical schemes validation. Cheol-Hee Ahn; supervision and result validation. Sarawut Rimdusit; supervision, resources, validation, review and editing.

Conflicts of interest

There are no conflicts to declare.

Acknowledgements

The authors would like to acknowledge and appreciate the support provided by the Second Century Fund (C2F) of Chulalongkorn University, Thailand. The authors would like to also express their sincere appreciation to the National Research Council of Thailand (NRCT) fund (No. 42A660910) and the Thailand Science Research and Innovation fund Chulalongkorn University (6641/2566).

Notes and references

1 B. Mekuye and B. Abera, Nanomaterials: An overview of synthesis, classification, characterization, and applications, *Nano Sel.*, 2023, **4**, 486–501.
2 V. Scardaci, Laser synthesized graphene and its applications, *Appl. Sci.*, 2021, **11**(14), 6304.
3 M. Chakraborty & M. S. J. Hashmi, Graphene as a Material – An Overview of Its Properties and Characteristics and Development Potential for Practical Applications, *Reference Module in Materials Science and Materials Engineering*, Elsevier Ltd, 2018, DOI: 10.1016/b978-0-12-803581-8.10319-4.
4 J. Lin, *et al.*, commercial polymers, *Nat. Commun.*, 2014, **5**, 12, DOI: 10.1038/ncomms6714.
5 Z. Zhang, *et al.*, A review of laser-induced graphene: From experimental and theoretical fabrication processes to emerging applications, *Carbon*, 2023, **214**, 118356.
6 L. Cao, *et al.*, Stable and durable laser-induced graphene patterns embedded in polymer substrates, *Carbon*, 2020, **163**, 85–94.

7 I. Lawan, P. Luengrojanakul, K. Charoensuk and H. Argunam, Laser-Induced Graphitization of Thermosetting Polymer Substrate and its Application—A Review, *Eng. J.*, 2023, **27**(10), 11–20.
8 A. P. Torlon, *6 Polyimides*, 2012, DOI: **10.1016/B978-1-4557-2598-4.00006-X**.
9 J. Hu, *et al.*, Preparation and characterization of luminescent polyimide/glass composite fiber, *J. Mater. Res. Technol.*, 2022, **18**, 4329–4339.
10 C. P. Constantin, M. Aflori, R. F. Damian & R. D. Rusu *Constantin 2019.Pdf*. 2019.
11 M. Usman, A. T. Jafry, A. Abbas, G. Hussain and N. Abbas, A high strength and flexible multilayered thin film laser induced graphene heater for thermal applications, *Thin Solid Films*, 2023, **780**, 139979.
12 S. A. A. Shah, R. Idrees and S. Saeed, A critical review on polyimide derived carbon materials for high-performance supercapacitor electrodes, *J. Energy Storage*, 2022, **55**, 105667.
13 D. X. Luong, *et al.*, Laser-Induced Graphene Composites as Multifunctional Surfaces, *ACS Nano*, 2019, **13**(2), 2579–2586.
14 J. T. Li, M. G. Stanford, W. Chen, S. E. Presutti and J. M. Tour, Laminated Laser-Induced Graphene Composites, *ACS Nano*, 2020, **14**, 7911–7919.
15 Y. Sui, *et al.*, Low temperature curing polyimides with covalent-boned 5-aminobenzimidazole, *Polyme*, 2021, **218**, 123514.
16 C. Huang, *et al.*, Comprehensive properties study of low-temperature imidized polyimide with curing accelerators, *J. Mater. Chem. C*, 2020, **8**, 14886–14894.
17 T. Takeichi, Y. Guo and S. Rimdusit, Performance improvement of polybenzoxazine by alloying with polyimide: Effect of preparation method on the properties, *Polymer*, 2005, **46**, 4909–4916.
18 K. S. Santhosh Kumar & C. P. Reghunadhan Nair, Polybenzoxazine-new generation phenolics, *Handb. Thermoset Plast*, 2014, pp. 45–73, DOI: **10.1016/B978-1-4557-3107-7.00003-8**.
19 S. Rimdusit, C. Jubsilp & S. Tiptipakorn, *Alloys and Composites of Polybenzoxazines:Properties and Applications*, Springer, 2013, vol. 13.
20 U. Misra, N. Dixit & S. P. Singh, *Effect of Laser Parameters on Laser-Induced Graphene Filter Fabrication and its Performance for Desalination and Water Purification*, 2023, DOI: **10.1021/acsami.2c17106**.
21 L. I. U. Ming, Effects of laser processing parameters on properties of laser- induced graphene by irradiating CO_2 laser on polyimide, *Sci. China: Technol. Sci.*, 2022, **65**, 41–52.
22 S. Bai *et al.*, *Investigation into the Influence of Interdigital Parameters on Electrochemical Performance for In-Plane Supercapacitors via Mathematical Modeling and Conformal Mapping Techniques*, 2023, vol. 65.
23 H. Wahab, *et al.*, Machine-learning-assisted fabrication : Bayesian optimization of laser- induced graphene patterning using in-situ Raman analysis, *Carbon*, 2020, **167**, 609–619.
24 T. Pinheiro, Influence of CO_2 laser beam modelling on electronic and electrochemical properties of paper-based laser-induced graphene for disposable pH electrochemical sensors, *Carbon Trends*, 2023, **11**, 100271.
25 S. Lamidi, N. Olaleye, Y. Bankole, A. Obalola, E. Aribike and I. Adigun, *Applications of Response Surface Methodology (RSM) in Product Design, Development*, John Wiley & Sons, 2005.
26 A. A. Younis, Evaluation of the flammability and thermal properties of a new flame retardant coating applied on polyester fabric, *Egypt. J. Pet.*, 2016, **25**, 161–169.
27 A. Velasco, *et al.*, Laser-Induced Graphene Microsupercapacitors: Structure, Quality, and Performance, *Nanomaterials*, 2023, **13**(5), 788.
28 T. M. Akintola, B. K. Kumar and T. Dickens, Combined Additive and Laser-Induced Processing of Functional Structures for Monitoring under Deformation, *Polymers*, 2023, **15**(2), 443.
29 Y. Wang, *et al.*, Laser direct writing of graphene photodetector with a wide spectral detection from the visible to the infrared, *Carbon Trends*, 2023, **11**, 100255.
30 Y. Yen *et al.*, *Laser-Induced Graphene Stretchable Strain Sensor with Vertical and Parallel Patterns*, 2022, vol. 1–14.
31 L. Cao, *et al.*, Stable and durable laser-induced graphene patterns embedded in polymer substrates, *Carbon*, 2020, **163**, 85–94.
32 Z. Yu, *et al.*, Upcycling of Polybenzoxazine to Magnetic Metal Nanoparticle-Doped Laser-Induced Graphene for Electromagnetic Interference Shielding, *ACS Appl. Nano Mater.*, 2022, **5**, 13158–13170.
33 B. Report, P. Ragulis, K. Ratautas & R. Trusovas, *Laser-Induced Graphene in Polyimide for Antenna Applications*, 2023.
34 J. Rodrigues *et al.*, *Nanoscale Advances by Direct Laser Scribing*, 2019, pp. 3252–3268, DOI: **10.1039/c8na00391b**.
35 I. R. Hristovski *et al.*, *Manifestations of Laser-Induced Graphene under Ultraviolet Irradiation of Polyimide with Varied Optical Fluence*, 2022.
36 D. Laser, *Sakarya Univ. J. Sci.*, 2023, **27**, 1105–1111.